Supporting Information

Brown et al. 10.1073/pnas.1504161112

SI Materials and Methods

Protein Purification. For ubiquitination assays, human APC, 3×Myc–His_6–CDH1, UBA1, UBE2S, UBCH5B, and donor Ub were purified as described (1, 2). Substrates were single-cysteine versions of CyclinB NTD* (residues 1–95), Ub–CyclinB NTD* (residues 1–95), Securin*, Ub–Securin*, Hsl1 (residues 768–842 and variants thereof), and acceptor Ub* (residues 1–74 G75S: G76S:C77) that were purified and fluorescently labeled, as denoted by an asterisk (*), with fluorescein-5 maleimide as described previously (1, 2).

Wild-type and mutant variants of UBCH10 used in APC substrate ubiquitination assays, oxyester-linked E2∼Ub discharge assays, and cross-linking for cryo-EM complexes were expressed in BL21 (DE3) Codon Plus (RIL) *Escherichia coli* cells and purified by nickel affinity chromatography based on a C-terminal His_6 tag. These variants were further purified by size exclusion chromatography (SEC) with buffer containing 20 mM Hepes, pH 8.0, 200 mM NaCl, and 1 mM DTT. The UBCH10∼Ub oxyester-linked complex for discharge assays was generated by incubating UBCH10 C114S (active-site mutation), UBA1, MgCl, ATP, and Ub at concentrations of 560 μM, 2 μM, 5 mM, and 3 mM, respectively, at 30 °C overnight. The UBCH10∼Ub oxyester-linked complex was separated from the other reaction components by SEC.

$UBCH10^{cat}$ (residues 27–179), APC2 WHB ($APC2^W$, residues 735–822), CUL1 WHB ($CUL1^W$, residues 702–776), and CUL2 WHB ($CUL2^W$, residues 664–745) were expressed as N-terminal GST fusions in BL21 (DE3) Gold *E. coli*. Ub (residues 1–74 G75C) and UbK_0 (all lysine residues mutated to arginines and a single cysteine immediately upstream of the N-terminal Met) were expressed as N-terminal GST fusions in BL21 (DE3) Codon Plus (RIL). These proteins were purified by glutathione affinity chromatography (3, 4), followed by removal of GST by either TEV or thrombin-mediated proteolysis. Subsequent purification steps included dialysis, removal of GST with glutathione Sepharose, and SEC. The final buffer conditions were 20 mM Hepes, pH 8.0, 200 mM NaCl, 1 mM DTT except for UBCH10 and $APC2^W$ used in crystallization, which were purified in 20 mM Tris 7.6, 150 mM NaCl, and 1 mM DTT. $*UbK_0$ was fluorescently labeled with fluorescein-5 maleimide as previously described (1, 2).

For NMR experiments, we used methods similar to those described previously for APC11 (1) to express $UBCH10^{cat}$ and $APC2^W$ in BL21 (DE3) Gold *E. coli* in minimal media. $APC2^W$ was prepared in the same manner as unlabeled proteins described above. $UBCH10^{cat}$ for NMR was expressed as the full-length protein with a N-terminal His_6, a C114S mutation, and an HRV13 3C protease site inserted at residue 27. After nickel affinity purification, the elution was treated with GST_HRV13 3C protease overnight followed by GST removal with glutathione Sepharose, and then buffer exchanged into 20 mM sodium phosphate, pH 6.0, 100 mM NaCl, and 10 mM DTT with NAP-5 column (GE Healthcare), and further concentrated in a high M_r centrifugal concentrator to remove excess UBCH10 N-terminal peptide.

APC-Dependent Substrate Ubiquitination Assays. The qualitative APC-mediated ubiquitination assays were performed as previously described (1, 2). In all APC-mediated ubiquitination experiments, except in Fig. S8, the substrate is fluorescently labeled and monitored for ubiquitination. In the APC-dependent ubiquitination of Hsl1 variants depicted in Fig. S8, the UbK_0 is fluorescently labeled at the N terminus and UbK_0 transfer was monitored during a time course. For all kinetic analyses, ubiquitination product bands were quantitated based on the fluorescein label on the substrate using a Typhoon FLA 9500 PhosphorImager. APC-independent ubiquitination products were subtracted as background to determine the APC-dependent activity.

The fitting of the initial velocities to the hyperbolic Michaelis–Menten, $v = V_{max}^{app}[X]/(K_m^{app} + [X])$, equation using GraphPad Prism 6 software, X represents the concentration of UBCH10, allowed for the determination of the apparent K_m (K_m^{app}) and apparent V_{max} (V_{max}^{app}) values for UBCH10-mediated ubiquitination activity with the APC. Single time points were used under conditions that satisfy initial velocity regimes (1). In summary, the K_m^{app} and V_{max}^{app} of UBCH10 was determined by titrating UBCH10 against 25 nM of either APC or APC (ΔAPC2 WHB) supplemented 1 μM CDH1, 2.5 μM Securin*, 5 mM $MgCl_2$, 5 mM ATP, 0.25 mg/mL BSA, and 0.1 μM UBA1. The reactions were initiated by the addition of 0.2 mM Ub and subsequently quenched at 10 min.

To determine the apparent inhibitor constant (K_i^{app}) of $APC2^W$ toward APC^{CDH1}–UBCH10-mediated Cyclin B NTD* ubiquitination, the initial velocities were fit to the Morrison quadratic function (below) using GraphPad Prism 6 software,

$$E_{free} = [E_0] - \frac{[E_0] + [I_0] + K_i^{app} - \sqrt{\left([E_0] + [I_0] + K_i^{app}\right)^2 - (4[E_0][I_0])}}{2},$$

where $[E_0]$ is the total enzyme concentration, $[I_0]$ is the total inhibitor concentration, and E_{free} is the concentration of free enzyme determined by the residual APC^{CDH1} activity against the activity and concentration of the uninhibited APC^{CDH1} activity. Various concentrations of $APC2^W$ were titrated by addition to 10 nM APC, 5 mM $MgCl_2$, 5 mM ATP, 0.25 mg/mL BSA, 0.5 μM Cyclin B1 NTD*, 1 μM CDH1, 0.1 μM E1, and 0.2 μM E2. Ub at 0.2 mM was added to initiate the reactions. These reactions were subsequently quenched at 10 min.

Preparation of APC^{CDH1}–UBCH10–Ub–Hsl1 Peptide Complex for Cryo-EM. To trap a complex representing APC in action, we first identified an optimal target lysine in a substrate derived from the high-affinity, KEN- and D-box–containing APC^{CDH1} substrate Hsl1 from *Saccharomyces cerevisiae* (Fig. S1) (5–8). Briefly, variants of a fragment of Hsl1 corresponding to residues 768–842 were generated with only two lysines, the Lys775 in the KEN-box and one other native lysine, and with all other lysines replaced by arginines. These were assayed for modification by APC^{CDH1} and UBCH10, using fluorescently labeled UbK_0. Greatest activity was observed for the substrate bearing an acceptor Lys at position 788 (Fig. S1). Next, we generated a minimal 33-residue version of Hsl1 ($Hsl1^P$, corresponding to a mutant version of Linker 19 in Fig. S8) by peptide synthesis with the following sequence: acetyl-NKENEGPEYPTKIEXYLEEQKPKRAALSDITNS-NH_2, where "X" is azidohomoalanine at the position corresponding to Lys788 using methods similar to those described previously (9). The azidohomoalanine served as the site of attachment of a custom-synthesized homobifunctional cross-linker similar to that we used previously to trap a HECT E3 as if in the act of transferring Ub to a substrate (9), except with a variant cross-linker generated as described below.

General chemical methods. All commercial reagents were used without further purification. All reactions were monitored by TLC carried out on EMD Chemicals silica gel 60-F254 coated glass plates and visualized using I_2 or UV light (254 nm). Analysis

by liquid chromatography–MS was performed by using an XBridge C_{18} column run at 1 mL/min, and using gradient mixtures of (A) water (0.05% TFA) and (B) methanol. Low-resolution mass spectra (electrospray ionization) were collected on a Waters Micromass ZQ in positive-ion mode. Flash chromatography was performed on a Biotage SP4 chromatography system using Biotage Flash KP-Sil. NMR spectra were obtained on BrukerAvance II NMR spectrometer at 400 MHz for 1H-NMR spectra. Chemical shifts (in parts per million) are reported relative to tetramethylsilane or the solvent peak. Signals are designated as follows: s, singlet; d, doublet; dd, doublet of doublet; t, triplet; q, quadruplet; m, multiplet. Coupling constants (J) are shown in hertz.

Abbreviations are as follows: DCM, dichloromethane; TEA, triethylamine; TES, triethylsilane; TFA, trifluoroacetic acid; THF, tetrahydrofuran.

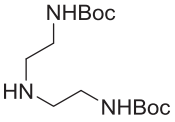

Preparation of di-tert-butyl (azanediylbis(ethane-2,1-diyl))dicarbamate. TEA (1.22 mL, 8.75 mmol) was added to a solution of diethylenetriamine (0.314 mL, 2.91 mmol) in THF (10 mL) at 0 °C. A solution of 2-(boc-oxyimino)-2-phenylacetonitrile (1.43 g, 5.81 mmol) in THF (5 mL) was added dropwise to the reaction mixture. After 1 h, the ice bath was removed and the reaction mixture stirred for 3 h at room temperature (RT). The reaction mixture was added to 0.1 M NaOH (50 mL) and extracted with ethyl acetate (3 × 50 mL). The combined organic layers were washed with saturated brine, dried over anhydrous Na_2SO_4, filtered, and concentrated. The crude product was purified by flash column chromatography [Biotage SP4, 40+M column, eluting with DCM:MeOH (1% NH_4OH), 0–10% gradient] to obtain the desired product (619 mg, 70% yield). ^{1}H NMR (400 MHz, chloroform-*d*) δ 4.92 (s, 2H), 3.49 (s, 1H), 3.22 (q, J = 5.8 Hz, 4H), 2.73 (t, J = 5.8 Hz, 4H), 1.45 (s, 18H).

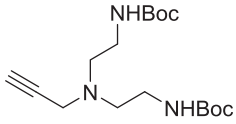

Preparation of di-tert-butyl ((prop-2-yn-1-ylazanediyl)bis(ethane-2,1-diyl)) dicarbamate. A solution of di-*tert*-butyl (azanediylbis(ethane-2,1-diyl)) dicarbamate (617 mg, 2.03 mmol), K_2CO_3 (281 mg, 2.03 mmol), and propargyl bromide (205 μL, 1.85 mmol), in acetone (5 mL), were heated to reflux and stirred overnight. The cooled reaction mixture was filtered, concentrated, and purified by flash column chromatography (Biotage SP4, 40+S column, eluting with hexanes:EtOAc, 0–50% gradient) to obtain the desired product (549 mg, 87% yield). ^{1}H NMR (400 MHz, chloroform-*d*) δ 4.89 (br s, 2H), 3.40 (d, J = 2.4 Hz, 2H), 3.20 (q, J = 5.8 Hz, 4H), 2.63 (t, J = 5.9 Hz, 4H), 2.19 (t, J = 2.3 Hz, 1H), 1.45 (s, 18H).

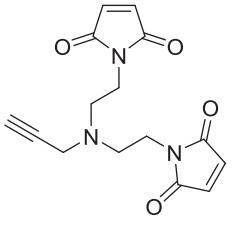

Preparation of 1,1′-((prop-2-yn-1-ylazanediyl)bis(ethane-2,1-diyl))bis(1H-pyrrole-2,5-dione). TFA (2.5 mL) was added to a solution of di-*tert*-butyl ((prop-2-yn-1-ylazanediyl)bis(ethane-2,1-diyl))dicarbamate (450 mg, 1.32 mmol) in DCM (2.5 mL) and TES (0.25 mL). The reaction mixture was concentrated after 1 h. Saturated $NaHCO_3$ (5 mL) was added and the mixture cooled to 0 °C. *N*-Methoxycarbonylmaleimide (443 mg, 2.86 mmol) was added portionwise to the stirring solution over the course of 15 min. After 3 h, the ice bath was removed and the reaction mixture stirred at RT for 1 h. The mixture was added to water (30 mL) and extracted with ethyl acetate (3 × 30 mL). The combined organic layers were washed with saturated brine, dried over anhydrous Na_2SO_4, filtered, and concentrated. The crude product was purified by flash column chromatography (Biotage SP4, 40+S column, eluting with hexanes:EtOAc, 0–100% gradient) to obtain the desired product as a white solid (344 mg, 78% yield). ^{1}H NMR (400 MHz, chloroform-*d*) δ 6.65 (s, 4H), 3.55 (t, J = 6.2 Hz, 4H), 3.50 (d, J = 2.4 Hz, 2H), 2.73 (t, J = 6.2 Hz, 4H), 2.17 (t, J = 2.3 Hz, 1H).

Procedure for click chemistry. (+)-Sodium L-ascorbate (120 μmol) was added portionwise to a solution of 1,1′-((prop-2-yn-1-ylazanediyl)bis(propane-3,1-diyl))bis(1H-pyrrole-2,5-dione) (120 μmol), the azidopeptide (30 μmol), and $CuSO_4$ (120 μmol), in H_2O/*t*BuOH (2:1, 20 mL). The solution was stirred for 1 h and then concentrated.

Purification of the Hsl1 peptide with homobifunctional sulfhydryl cross-linker. The crude peptide was dissolved in water:acetonitrile (90:10) and purified on a Waters 2695 semipreparative HPLC (Waters) using an XBridge C18, 5 μm, 250 × 10-mm column (Waters) over 45 min with a flow rate of 4 mL/min, and using a gradient of 0–50% B, where Buffer A is 0.1% TFA in water, and Buffer B is 0.1% TFA in acetonitrile. Detection was at 220 and 240 nm. Fractions containing the correct mass were analyzed on the analytical HPLC, pooled, and lyophilized. HPLC purity of the purified peptide was >99%, and correct mass was verified.

Purification of APC^{CDH1} in complex with three-way cross-linked UBCH10–Hsl1^P–Ub. First, a three-way cross-linked complex was formed between UBCH10–His_6 (C102A) and Ub (1–74, G75C) using methods described for a different peptide and cross-linker (Fig. 1 and Fig. S1) (9). Briefly, the proteins were treated with 10 mM DTT for 30 min before they were desalted into 50 mM Hepes 7.0, 150 mM NaCl. UBCH10–Ub–Hsl1^P was prepared by reacting the Ub with the Hsl1^P containing the two maleimide moieties at 1:1 Ub:peptide ratio for 20 min on ice. UBCH10 was then added at a 1:1 ratio for 1–2 h at RT. The reaction was quenched with 10 mM β-mercaptoethanol. After purification, intact mass spectrometry confirmed the three-way cross-linked complex (Hartwell Center for Biotechnology and Bioinformatics, St. Jude Children's Research Hospital, Memphis, TN). We adapted the previously described protocol for preparing an APC–UBE2S complex for EM to purify a complex between the three-way cross-linked UBCH10–Ub–Hsl1^P complex and APC^{CDH1} (1). The APC^{CDH1}–UBCH10–Ub–Hsl1^P complex was polished through GraFix for EM analysis (10).

Cryo-EM. The APC^{CDH1}–UBCH10–Ub–Hsl1^P complex (hereafter referred to as "APC^{CDH1}–UBCH10–Ub–substrate") was prepared on grids (Quantifoil 3.5/1 μm; Jena) covered with continuous carbon. Cryo-EM grids were prepared under controlled environmental conditions at 4 °C and 100% humidity in a vitrification device (Vitrobot Mark IV; FEI Company). A total of 2,097 image frames were recorded in spot-scanning mode (3 × 3 image frames per 3.5-μm hole) on a Falcon II direct detector under liquid-nitrogen conditions with a Titan Krios electron microscope (FEI) equipped with a XFEG electron source and a C_s corrector (CEOS) using 300-kV acceleration voltage, an electron dose of ∼30 ± 5 electrons per Å^2, −1.5- to −4-μm defocus, and a nominal magnification of 94,000×, resulting in a final pixel size of ∼1.57 Å. APC particle images were extracted in a fully automated manner using template-independent custom-made software (CowPicker, B. Busche and H.S.). The 550,217

extracted particle images were corrected locally for the contrast-transfer function (CTF) by classification and averaging (11), and selected according to quality of power spectra. The resulting 399,187 CTF-corrected particle images were further selected for contaminations (resulting in 338,932 particle images) and further sorted into groups of particles according to the presence or absence of the proteins APC7, APC2, and UBCH10, resulting in a final set of 47,791 particle images used in a refinement [with RELION (12)] to a resolution of 8 Å as defined by the "gold-standard" Fourier shell correlation procedure. Pymol and Chimera were used to generate figures of structures and EM density (13, 14).

Monitoring Hydrolysis of Oxyester-Linked Analog of UBCH10~Ub to Assay Substrate-Independent APC-Dependent Activation. To determine the ability of APC complexes to activate UBCH10~Ub in the absence of substrates, we used an oxyester-linked version of the UBCH10~Ub complex where Ub's C terminus is linked to a serine substituted for the catalytic Cys114 of UBCH10. The oxyester-linked UBCH10(C114S)~Ub was mixed with either wild-type or variant versions of APC2–APC11, or APC in the absence or presence of CDH1. Experiments were performed at RT and monitored the persistence of E2~Ub and generation of the hydrolytic products UBCH10 and Ub over time. Reaction mixtures contained 20 μM UBCH10~Ub and 1 μM wild-type or variant versions of APC. APC2–APC11 complexes could be made in larger quantity, and therefore experiments could be performed with a higher concentration (10 μM) of APC2–APC11 and variants. As expected, this increase in E3 concentration promoted hydrolysis of oxyester-linked UBH10~Ub in a shorter time frame. Reaction products were separated by SDS/PAGE and visualized by staining with Coomassie blue.

$APC2^W$ Inhibition of E1-Catalyzed Generation of an UBCH10~Ub Conjugate. Reactions were performed by mixing 5 mM $MgCl_2$, 5mM ATP, 0.25 mg/mL BSA, and 0.1 μM E1, 2 μM E2, and $APC2^W$. These reactions were then initiated by adding 4 μM fluorescently labeled UbK_0. The reactions were then quenched over a time course. The products were separated by SDS/PAGE and monitored by fluorescent scanning and SYPRO Ruby protein staining.

Assays Monitoring Degradation of APC Substrates in *Xenopus* Egg Extracts. Interphase egg extracts were prepared and APC-dependent degradation of Cyclin B and Securin was triggered by adding nondegradable cyclin B (Δ90) at 300 nM for 120 min before assay largely as previously described (2, 15–17). Two types of assays were performed. To test the effects of deleting domains from APC, extracts were immunodepleted of endogenous APC by mixing 70 μL of interphase extract with 2.5 μg of anti-APC3 antibody coupled to 10.5 μL of Affiprep Protein A beads and incubating at 4 °C for 40 min, twice. APC activity was restored as described previously, by adding recombinant human APC to the extracts (2). Approximately 1.05 μg of recombinant APC/C complex was added to 15 μL of APC/C-depleted extract. Reactions were incubated at 22 °C for the indicated times after recombinant human Securin and Cyclin B1/CDK1 addition, and the reactions were quenched with SDS/PAGE sample buffer and boiled for 3 min.

To test whether the isolated $APC2^W$ could interfere with APC activity by competing for UBCH10 binding, the indicated amounts of purified APC2 WHB domain were added to activated extracts, and degradation of the added Cyclin B1 and Securin was monitored over time.

NMR Spectroscopy.

NMR sample conditions and assignments. Assignment of $APC2^W$ domain resonances was carried out at 298 K using a uniformly ^{13}C,^{15}N-labeled sample with a concentration of 500 μM, and were performed in a 20 mM sodium phosphate buffer (pH 7.0) with 100 mM NaCl, 10 mM DTT, and 0.1% sodium azide in 90% H_2O/10% D_2O. Titration experiments with UBCH10 were carried out on either ^{15}N-labeled or ^{13}C,^{15}N-labeled WHB samples at 100 μM concentration in the same buffer.

Assignment of $UBCH10^{cat}$ resonances was carried out at 298 K using a uniformly labeled ^{13}C,^{15}N-labeled sample with a concentration of 500 μM and were performed in a 20 mM sodium phosphate buffer (pH 6.0) with 100 mM NaCl, 10 mM DTT, and 0.1% sodium azide solved in 90% H_2O/10% D_2O. Titration experiments with $APC2^W$ were carried out on either uniformly ^{15}N-labeled or ^{13}C, ^{15}N-labeled or perdeuterated ^{13}C,^{15}N-labeled $UBCH10^{cat}$ C114S mutant at 100 μM concentration in the same buffer.

Backbone assignments of free $UBCH10^{cat}$, $APC2^W$, and their complexes. NMR experiments were measured on either a Bruker 600- or 800-MHz spectrometer equipped with a ^1H and ^{13}C detect, TCI triple resonance cryogenic probe using standard Bruker pulse programs. ^1H, ^{13}C, and ^{15}N backbone resonances of free WHB were assigned using standard triple-resonance heteronuclear single-quantum coherence (HSQC)-based experiments, such as HNCA, HNCACB, CBCA(CO)NH, HNCO, and HN(CA)CO. Because the resonances in the binding pocket could not be traced from titrations, the backbone resonances of WHB domain in complex with UBCH10 was assigned using HNCA, HNCO, and HN(CA)CO TROSY-based 3D experiments. Similarly, for the backbone resonance assignment of UBCH10, the 3D data were collected on three different constructs. Initially uniformly labeled ^{13}C,^{15}N-UBCH10 full-length sample was prepared in 20 mM Hepes 7.0, 100 NaCl, 10 mM DTT, and both HSQC- and TROSY-based 3D HNCA, HNCACB, CBCA(CO)NH spectra were collected. Because of the poor signal-to-noise in the spectra, only 50% of the resonances could be assigned without ambiguity. Then the same data were collected on the uniformly labeled ^{13}C,^{15}N-UBCH10 sample, without the first 26 residues of N-terminal, which was unstructured. Although signal to noise in this construct improved, it was difficult to assign more than 60% of the observed resonances. Hence the following TROSY-based experiments were collected: HNCA, HNCACB, HN(CO)CACBNH, HNCO, and HN(CA)CO on perdeuterated ^{13}C,^{15}N-$UBCH10^{cat}$ C114S mutant sample in the same buffer at 298 K. The resonances of the $UBCH10^{cat}$–WHB complex were confirmed using TROSY-based 3D HNCA and ^{15}N-resolved 3D [^1H, ^1H] NOESY spectra, which were also collected on free UBCH10 sample. All of the ^1H chemical shifts were referenced with respect to 4,4-dimethyl-4-silapentane-1-sulfonic acid (DSS) measured in the same buffer, whereas the ^{13}C and ^{15}N chemical shifts were referenced indirectly with respect to the DSS shift.

Heteronuclear NOE data on free UBCH10 as well as its complex with WHB domain were also collected on perdeuterated ^{13}C,^{15}N-labeled UBCH10 C114S mutant using 3-s saturation time and a recycle delay of 2.5 s with 40 scans.

All of the spectra were processed using topspin software and analyzed using the computer-aided resonance software, CARA (18). Random coil chemical shifts for the secondary structure calculations of both WHB and UBCH10 were obtained using the online prediction method (19). Chemical shift perturbations for the complexes were calculated using the formula $((\Delta H)^2 + 0.5*(\Delta N)^2)^{0.5}$, where ΔH and ΔN correspond to the difference in the chemical shifts for free and bound proton and nitrogen resonances, respectively.

X-Ray Crystallography. $UBCH10^{cat}$ and $APC2^W$ were mixed together to a final concentration of 0.2 mM and mixed with reservoir solutions at a 1:1 volume:volume ratio for crystallization by the hanging-drop vapor diffusion method. The reservoir solution contained 0.1 M Mes, pH 6.5, 35% PEG 3000. The reservoir solution was supplemented with 20% glycerol to serve as a cryoprotectant during the flash-freezing process with liquid nitrogen before data collection at NECAT 24-ID-C. Diffraction

data were processed with HKL2000 (20). The structure was determined by molecular replacement using Phaser with UBCH10 [Protein Data Bank (PDB) ID code 1I7K] and the yeast APC2^{W} domain (PDB ID code 1LDD) with sequence changed to polyalanine as search models (21–23). Model construction and refinement was performed using Coot, Refmac5, and Phenix (24–26). Diffraction data and refinement statistics are provided in Table S1.

1. Brown NG, et al. (2014) Mechanism of polyubiquitination by human anaphase-promoting complex: RING repurposing for ubiquitin chain assembly. *Mol Cell* 56(2):246–260.
2. Yamaguchi M, et al. (2014) Structure of an APC3-APC16 complex: Insights into assembly of the anaphase-promoting complex/cyclosome. *J Mol Biol*, 10.1016/j.jmb.2014.11.020.
3. Huang DT, Zhuang M, Ayrault O, Schulman BA (2008) Identification of conjugation specificity determinants unmasks vestigial preference for ubiquitin within the NEDD8 E2. *Nat Struct Mol Biol* 15(3):280–287.
4. Monda JK, et al. (2013) Structural conservation of distinctive N-terminal acetylation-dependent interactions across a family of mammalian NEDD8 ligation enzymes. *Structure* 21(1):42–53.
5. Burton JL, Solomon MJ (2001) D box and KEN box motifs in budding yeast Hsl1p are required for APC-mediated degradation and direct binding to Cdc20p and Cdh1p. *Genes Dev* 15(18):2381–2395.
6. da Fonseca PC, et al. (2011) Structures of APC/C(Cdh1) with substrates identify Cdh1 and Apc10 as the D-box co-receptor. *Nature* 470(7333):274–278.
7. Schreiber A, et al. (2011) Structural basis for the subunit assembly of the anaphase-promoting complex. *Nature* 470(7333):227–232.
8. Buschhorn BA, et al. (2011) Substrate binding on the APC/C occurs between the co-activator Cdh1 and the processivity factor Doc1. *Nat Struct Mol Biol* 18(1):6–13.
9. Kamadurai HB, et al. (2013) Mechanism of ubiquitin ligation and lysine prioritization by a HECT E3. *eLife* 2:e00828.
10. Kastner B, et al. (2008) GraFix: Sample preparation for single-particle electron cryomicroscopy. *Nat Methods* 5(1):53–55.
11. Sander B, Golas MM, Stark H (2003) Automatic CTF correction for single particles based upon multivariate statistical analysis of individual power spectra. *J Struct Biol* 142(3):392–401.
12. Scheres SH (2012) RELION: Implementation of a Bayesian approach to cryo-EM structure determination. *J Struct Biol* 180(3):519–530.
13. Pettersen EF, et al. (2004) UCSF Chimera—a visualization system for exploratory research and analysis. *J Comput Chem* 25(13):1605–1612.
14. Schrodinger LLC (2010) The PyMOL Molecular Graphics System, Version 1.3r1 (Schrodinger, LLC, New York).
15. Shteinberg M, Protopopov Y, Listovsky T, Brandeis M, Hershko A (1999) Phosphorylation of the cyclosome is required for its stimulation by Fizzy/cdc20. *Biochem Biophys Res Commun* 260(1):193–198.
16. Lahav-Baratz S, Sudakin V, Ruderman JV, Hershko A (1995) Reversible phosphorylation controls the activity of cyclosome-associated cyclin-ubiquitin ligase. *Proc Natl Acad Sci USA* 92(20):9303–9307.
17. Félix MA, Labbé JC, Dorée M, Hunt T, Karsenti E (1990) Triggering of cyclin degradation in interphase extracts of amphibian eggs by cdc2 kinase. *Nature* 346(6282):379–382.
18. Keller RLJ (2004) *Computer Aided Resonance Assignment Tutorial.* Available at cara.nmr-software.org/downloads/3-85600-112-3.pdf. Accessed March 19, 2015.
19. Kjaergaard M, Brander S, Poulsen FM (2011) Random coil chemical shift for intrinsically disordered proteins: Effects of temperature and pH. *J Biomol NMR* 49(2):139–149.
20. Otwinowski Z, Minor W (1997) Processing of X-ray diffraction data collected in oscillation mode. *Methods Enzymol* 276:307–326.
21. Lin Y, Hwang WC, Basavappa R (2002) Structural and functional analysis of the human mitotic-specific ubiquitin-conjugating enzyme, UbcH10. *J Biol Chem* 277(24):21913–21921.
22. Zheng N, et al. (2002) Structure of the Cul1-Rbx1-Skp1-F boxSkp2 SCF ubiquitin ligase complex. *Nature* 416(6882):703–709.
23. McCoy AJ, et al. (2007) Phaser crystallographic software. *J Appl Cryst* 40(Pt 4):658–674.
24. Murshudov GN, Vagin AA, Dodson EJ (1997) Refinement of macromolecular structures by the maximum-likelihood method. *Acta Crystallogr D Biol Crystallogr* 53(Pt 3):240–255.
25. Emsley P, Lohkamp B, Scott WG, Cowtan K (2010) Features and development of Coot. *Acta Crystallogr D Biol Crystallogr* 66(Pt 4):486–501.
26. Adams PD, et al. (2010) PHENIX: A comprehensive Python-based system for macromolecular structure solution. *Acta Crystallogr D Biol Crystallogr* 66(Pt 2):213–221.

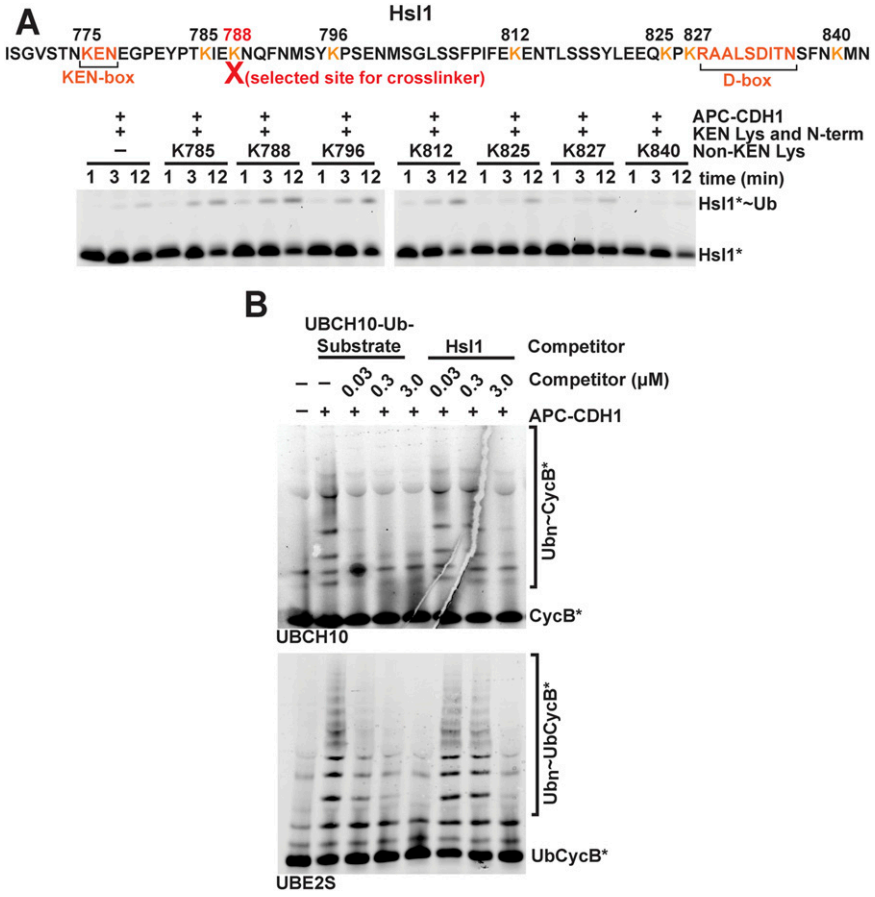

Fig. S1. Generation of a trapped complex representing APC^{CDH1}–UBCH10–Ub–substrate intermediate. (*A*) Identification of an optimal acceptor site in the high-affinity and well-characterized yeast substrate Hsl1. Monoubiquitination of various Hsl1 lysines by APC^{CDH1}, UBCH10, and UbK_0 was compared. Variants of an Hsl1 fragment comprising residues 768–842 harbor arginine replacements for all lysines except Lys775 in the KEN-box and one other lysine as indicated. The construct with Lys788 showed most ubiquitination. Thus, residue 788 was selected as the site to incorporate azidohomoalanine for modification with a bis-maleimide cross-linker. This enabled three-way cross-linking between a synthetic peptide derived from Hsl1 at the residue corresponding to position 788, UBCH10's catalytic cysteine, and a cysteine at a C-terminal residue 75 in a Ub mutant. (*B*) Representative fluorescent scans of ubiquitination assays testing whether the three-way cross-linked UBCH10–Ub–substrate complex properly binds APC^{CDH1}. If the cross-linked UBCH10–Ub–substrate complex binds both the substrate binding site via Hsl1 and the APC2–APC11 cullin–RING catalytic core via UBCH10–Ub, then the cross-linked UBCH10–Ub–substrate complex should inhibit APC^{CDH1}-catalyzed substrate ubiquitination at a lower concentration than Hsl1 does on its own. This was confirmed in assays for ubiquitination of Cyclin B* with UBCH10 (*Top*) or UbCyclin B* with UBE2S (*Bottom*).

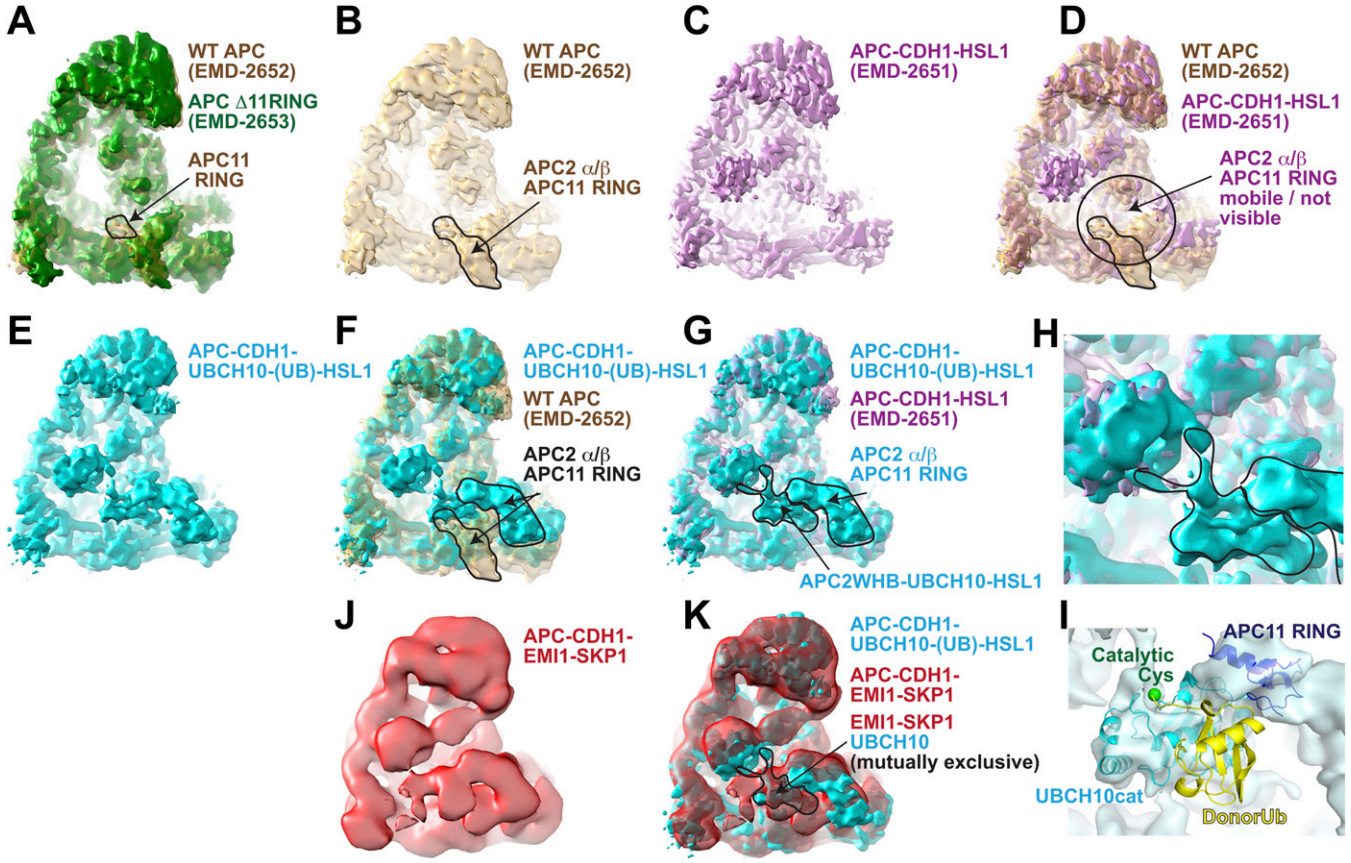

Fig. S2. Insights into APC regulation and activity by comparing cryo-EM maps of various complexes. (*A*) A prior study compared cryo-EM maps for APC (tan) and APC lacking APC11's RING domain (ΔRING, green) to identify location of RING domain (1). (*B*) Location of APC2–APC11 interaction α/β-domain and RING domain outlined on EM map of apo-APC based on prior study (1). (*C*) Prior EM map of APC^{CDH1}–substrate complex is shown in violet (1). (*D*) Prior studies showed substantial conformational changes to the APC catalytic core (APC2–APC11) and flanking subunits (APC1, APC4, APC5) upon binding to CDH1 and Hsl1 substrate (violet) (1). Circle shows that neither APC11 nor APC2's C-terminal domains are visible in the prior refined map of an APC^{CDH1}–Hsl1 complex (1). (*E*) EM map of APC^{CDH1}–UBCH10–Ub–substrate complex from this work is shown in cyan. (*F*) Superposition of EM maps for APC^{CDH1}–UBCH10–Ub–substrate complex (cyan) and apo APC (tan) (1) shows relocalization of APC catalytic core elements, APC11 and APC2's C-terminal domains (outlined). (*G*) Superposition of EM maps for APC^{CDH1}–UBCH10–Ub–substrate complex (cyan) and APC^{CDH1}–substrate (violet) shows location of three-way cross-linked UBCH10–Ub–substrate complex (outlined). (*H*) Close-up of *G*, highlighting position of three-way cross-linked UBCH10–Ub–substrate complex adjacent to APC2–APC11 interaction α/β-domain and RING domain. (*I*) Cryo-EM reconstruction of the APC^{CDH1}–UBCH10–Ub–substrate complex, showing $UBCH10^{cat}$ structure docked with APC11 RING domain and donor Ub by superimposing a homologous RING–E2~Ub structures (2, 3), fit into the EM map using Chimera (4). (*J*) EM map of APC^{CDH1}–EMI1–SKP1 complex is shown in red (5). (*K*) Superposition of EM maps for APC^{CDH1}–UBCH10–Ub–substrate complex (cyan) and APC^{CDH1}–EMI1–SKP1 (red) (5) shows that EMI1–SKP1 and UBCH10 binding to APC is mutually exclusive.

1. Chang L, Zhang Z, Yang J, McLaughlin SH, Barford D (2014) Molecular architecture and mechanism of the anaphase-promoting complex. *Nature* 513(7518):388–393.
2. Plechanovová A, Jaffray EG, Tatham MH, Naismith JH, Hay RT (2012) Structure of a RING E3 ligase and ubiquitin-loaded E2 primed for catalysis. *Nature* 489(7414):115–120.
3. Dou H, Buetow L, Sibbet GJ, Cameron K, Huang DT (2012) BIRC7-E2 ubiquitin conjugate structure reveals the mechanism of ubiquitin transfer by a RING dimer. *Nat Struct Mol Biol* 19(9): 876–883.
4. Pettersen EF, et al. (2004) UCSF Chimera—a visualization system for exploratory research and analysis. *J Comput Chem* 25(13):1605–1612.
5. Frye JJ, et al. (2013) Electron microscopy structure of human APC/C(CDH1)-EMI1 reveals multimodal mechanism of E3 ligase shutdown. *Nat Struct Mol Biol* 20(7):827–835.

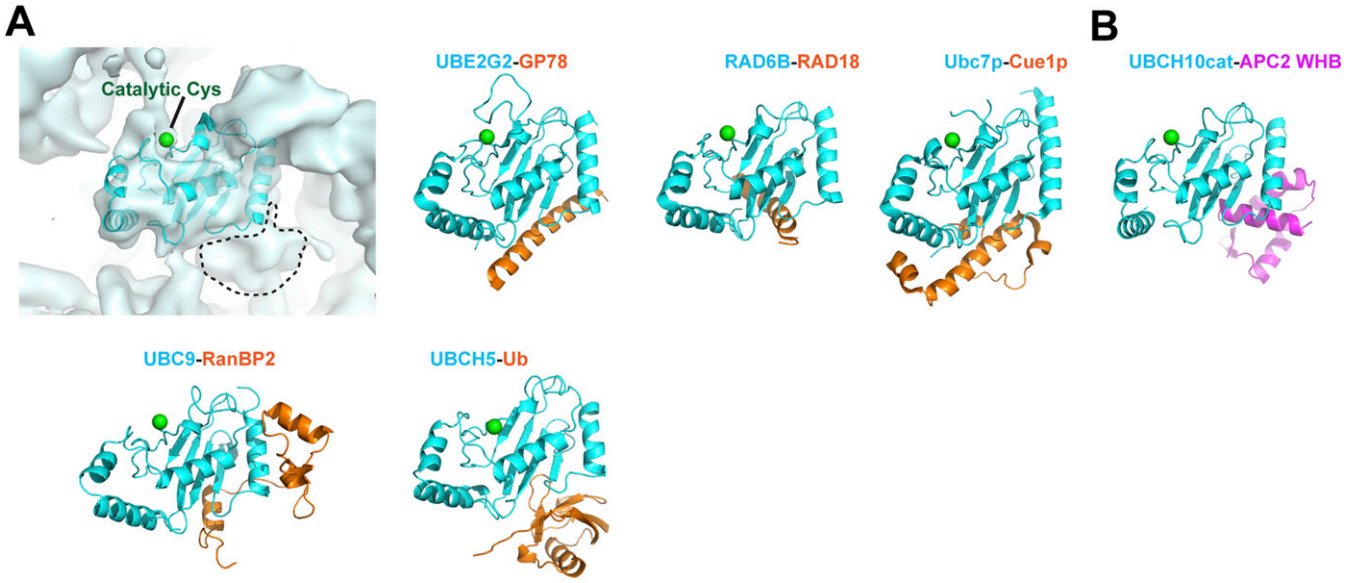

Fig. S3. E2 backside interactions. (*A*) Fitting UBCH10 catalytic domain into cryo-EM density for trapped complex representing APC^{CDH1}–UBCH10–Ub–substrate intermediate showed a domain contacting the "backside" of UBCH10, opposite the active site harboring the catalytic cysteine. This is shown aligned with structures of five different E2s (cyan) in complexes with their distinctive backside binding partners (orange): UBE2g2–GP78 (3H8K.pdb) (1); RAD6B–RAD18 (2YBF.pdb) (2); Ubc7p–Cue1p (4JQU.pdb) (3); UBC9–RanBP2 (RanGAP1 and SUMO-1 not shown; 1Z5S.pdb) (4); and UBCH5–Ub (2FUH.pdb) (5). (*B*) Crystal structure of $UBCH10^{cat}$–$APC2^{W}$ complex shows the WHB domain from APC2 (magenta) bound to the backside of UBCH10.

1. Das R, et al. (2009) Allosteric activation of E2-RING finger-mediated ubiquitylation by a structurally defined specific E2-binding region of gp78. *Mol Cell* 34(6):674–685.
2. Hibbert RG, Huang A, Boelens R, Sixma TK (2011) E3 ligase Rad18 promotes monoubiquitination rather than ubiquitin chain formation by E2 enzyme Rad6. *Proc Natl Acad Sci USA* 108 (14):5590–5595.
3. Metzger MB, et al. (2013) A structurally unique E2-binding domain activates ubiquitination by the ERAD E2, Ubc7p, through multiple mechanisms. *Mol Cell* 50(4):516–527.
4. Reverter D, Lima CD (2005) Insights into E3 ligase activity revealed by a SUMO-RanGAP1-Ubc9-Nup358 complex. *Nature* 435(7042):687–692.
5. Brzovic PS, Lissounov A, Christensen DE, Hoyt DW, Klevit RE (2006) A UbcH5/ubiquitin noncovalent complex is required for processive BRCA1-directed ubiquitination. *Mol Cell* 21(6):873–880.

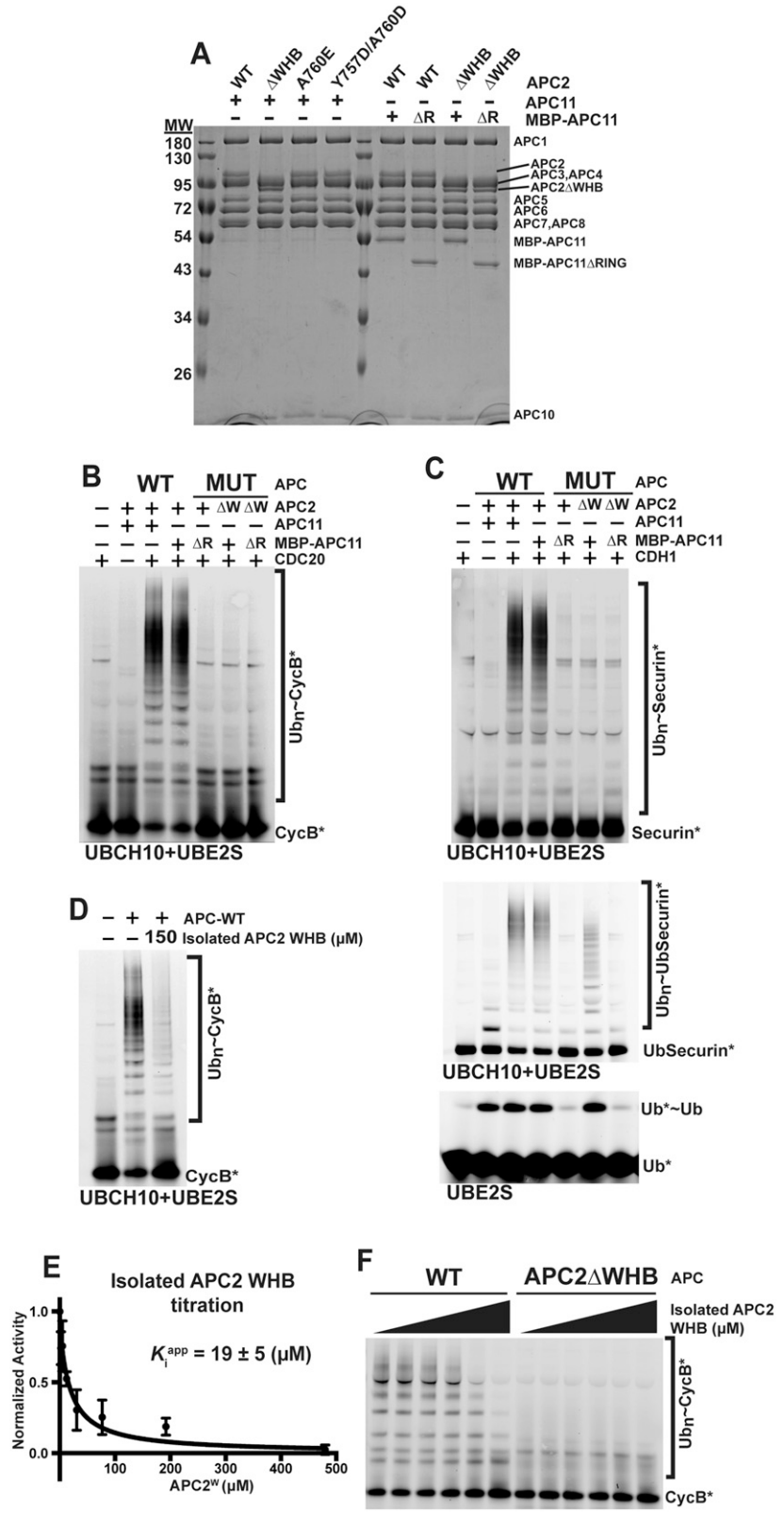

Fig. S4. Representative raw data and curve fitting demonstrating that the APC2 WHB domain is essential for substrate ubiquitination by APC^{CDH1} and APC^{CDC20} with UBCH10. (*A*) Coomassie-stained SDS/PAGE gel of purified APC variants used in biochemical studies. Note that experiments comparing activities of APC11 mutants contain His_6–MBP–APC11 to detect stoichiometric incorporation. (*B*) Fluorescence scan of assay testing effects of deleting APC2's WHB domain (ΔW) and/or the APC11's RING domain (ΔR) on fluorescent Cyclin B (CycB*) ubiquitination by APC^{CDC20} with both E2s UBCH10 and UBE2S together. In these reactions, APC^{CDC20} and UBE2S extend Ub chains initiated by APC^{CDC20} and UBCH10. (*C*) Fluorescence scans of ubiquitination assays testing E2 specificity for effects of deleting APC2's WHB domain (ΔW) and/or the APC11's RING domain (ΔR). Assays show ubiquitination of Securin* (*Top*) and UbSecurin* (*Middle*) by

Legend continued on following page

APC^{CDH1} with both UBCH10 and UBE2S (together), or on di-Ub synthesis by the indicated versions of APC^{CDH1} and UBE2S. The data, together with that in Figs. 2 and 3, and Figs. S5 and S6, show that the defect caused deleting APC2's WHB domain is specific for UBCH10 activity. (*D*) Experiments testing whether the isolated APC2 WHB ($APC2^{W}$) could inhibit ubiquitination of CycB* by APC^{CDH1} with both UBCH10 and UBE2S together. In these reactions, APC^{CDH1} and UBE2S extend Ub chains initiated by APC^{CDH1} and UBCH10. (*E*) Curve fits measuring the apparent K_i (K_i^{app}) for $APC2^{W}$ inhibition of CycB* ubiquitination by APC^{CDH1} and UBCH10. SEM, $n \geq 3$. (*F*) Experiments testing whether adding the isolated $APC2^{W}$ compensates for defective Cyclin B ubiquitination by APC^{CDH1} lacking APC2's WHB domain (APC2ΔWHB). Compensation is not observed. Instead, the data show dose-dependent inhibition of wild-type APC^{CDH1}, but no effect on the APC2ΔWHB mutant.

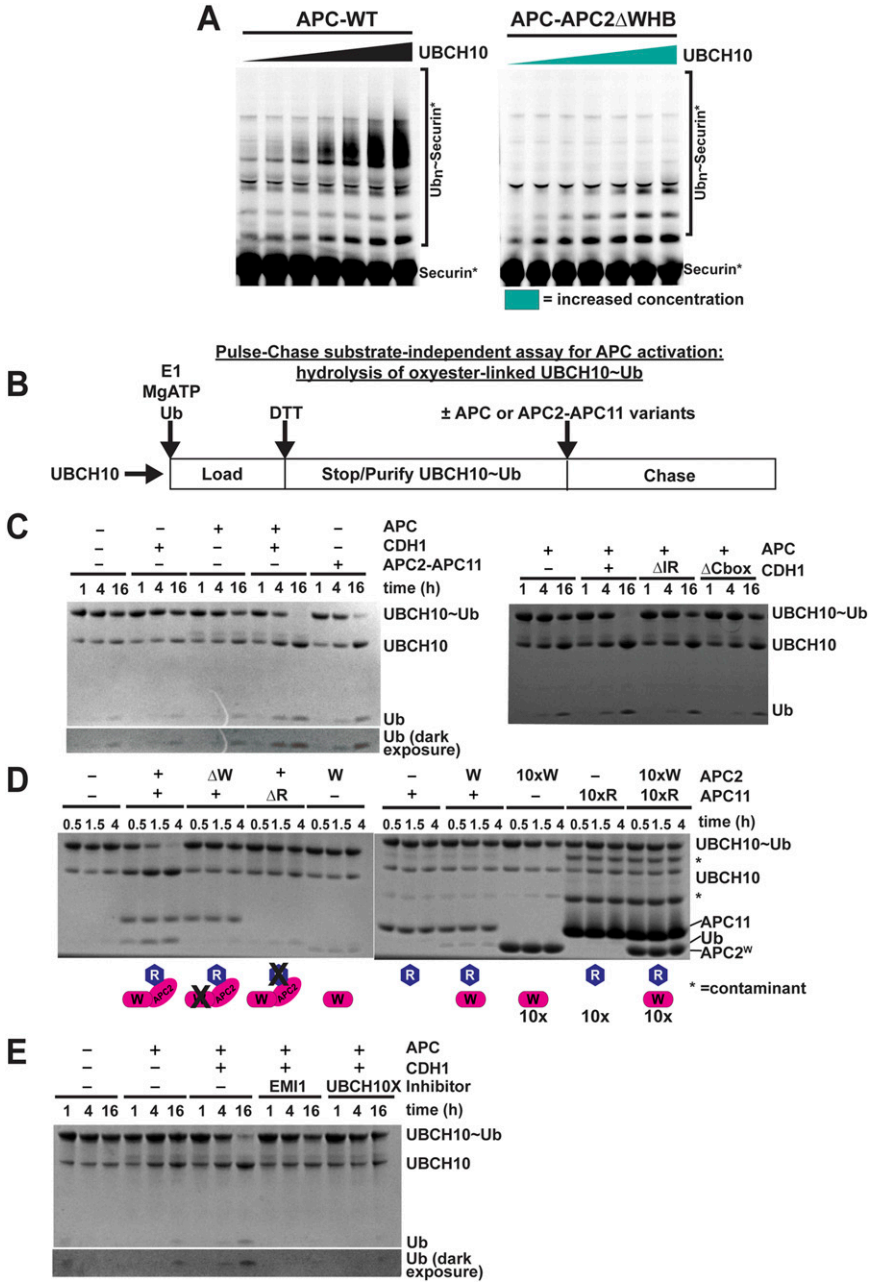

Fig. S5. Bipartite recruitment of UBCH10 to APC drives UBCH10-dependent ubiquitination. (*A*) Representative SDS/PAGE gels for data used to determine kinetic parameters in titrating UBCH10 concentration in assays measuring ubiquitination of fluorescent Securin* with either APC^{CDH1}–WT or APC^{CDH1}–APC2ΔWHB. (*B*) Schematic of assay for substrate-independent APC activation of UBCH10. The assay is performed in two-step pulse–chase format and monitors abilities of various wild-type and mutant APC complexes to stimulate hydrolysis of oxyester-linked UBCH10~Ub. First, the oxyester-linked UBCH10~Ub intermediate is generated in the pulse reaction. Here, a Ser replacement for UBCH10's active-site Cys114 was oxyester-bonded to Ub's C terminus in the reaction catalyzed by the E1 UBA1 in the presence of MgATP. The pulse Ub-loading reaction is quenched with DTT to prevent further E1 activity, and oxyester-linked UBCH10~Ub is purified by gel filtration. Second, the oxyester-linked UBCH10~Ub complex is hydrolyzed over time in the chase reaction. To test catalytic activity in the absence of ubiquitination substrates, various versions of APC or APC subcomplexes were added to UBCH10~Ub, in the presence or absence of the coactivator CDH1, and time points were taken to monitor E3-dependent hydrolysis of the UBCH10~Ub by SDS/PAGE and Coomassie staining. Upper portions of gels displaying APC and variants are not shown for simplification. (*C*) Pulse–chase assay for substrate-independent catalysis with UBCH10. (*Left*) Assay testing APC ± CDH1 or the isolated APC catalytic core (APC2–APC11 complex) for substrate-independent E3 activity. (*Right*) Assay testing roles of known catalytic elements from CDH1, the C-box, and IR-tail. Experiments were performed by adding 1 μM of the indicated versions of APC ± CDH1, or APC2–APC11, to stimulate hydrolysis with 20 μM UBCH10~Ub. Note that, due to the relatively lower concentration of APC, many reaction turnovers are required to observe hydrolysis by Coomassie detection. (*D*) Similar to *C*, but testing roles of APC2's WHB and/or APC11's RING domain on substrate-independent E3 activity for the catalytic core. APC2–APC11 variants included deletion of the WHB domain (ΔW) or deletion of APC11's RING domain (ΔR). Also, high concentrations of the isolated WHB domain from APC2 (W) and/or RING (R) domain from APC11 were assayed for ability to activate the oxyester-linked UBCH10~Ub complex. Experiments were performed with 1:2 ratios of APC2–APC11 (10 μM):UBCH10~Ub (20 μM) or with 5:1 ratios (100 μM) for the isolated domains as indicated (10x). The rate of hydrolysis is faster in these experiments compared with *C* because of the 10-fold higher concentration of APC2–APC11 that could be used in this experiment. (*E*) Similar to *C*, but testing abilities of the cross-linked UBCH10–Ub–substrate complex used in EM studies (UBCH10X) and EMI1–SKP1 to inhibit substrate-independent APC^{CDH1} activation of UBCH10~Ub.

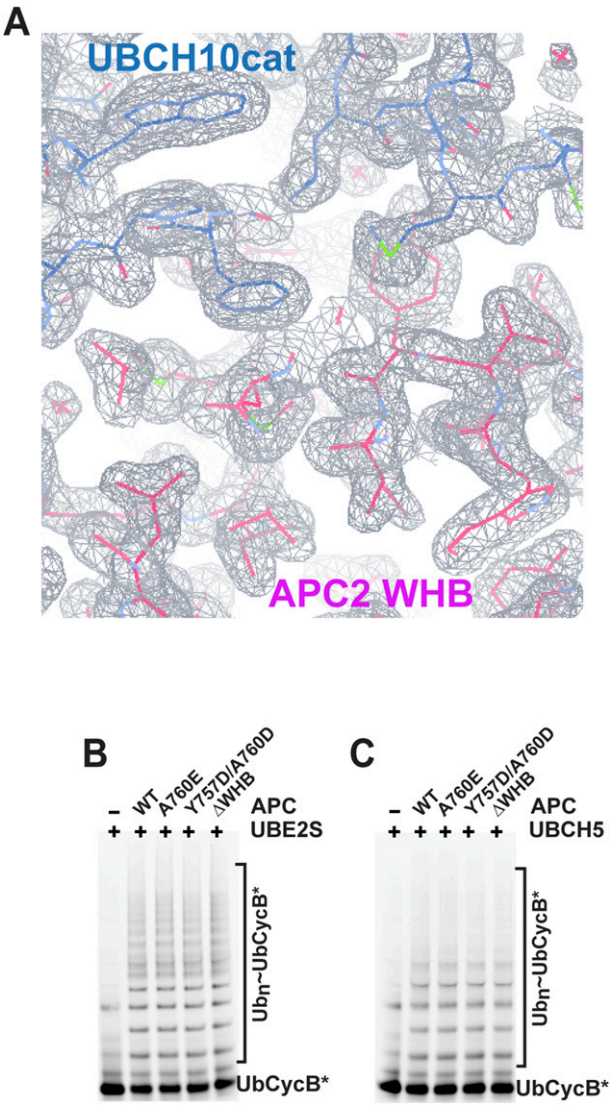

Fig. S6. Crystal structure shows basis for specific interactions between APC2 and UBCH10. (*A*) Final $2F_o - F_c$ electron density contoured at 1σ over a portion of the $APC2^{W}$–$UBCH10^{cat}$ interface. (*B*) Control reactions for Fig. 4*C*, showing effects of APC2 point mutations in residues contacting UBCH10 on APC^{CDH1}–UBE2S-dependent ubiquitination of UbCycB*. (*C*) Control reactions for Fig. 4*C*, showing effects of APC2 point mutations in residues contacting UBCH10 on APC^{CDH1}–UBCH5-dependent ubiquitination of UbCycB*.

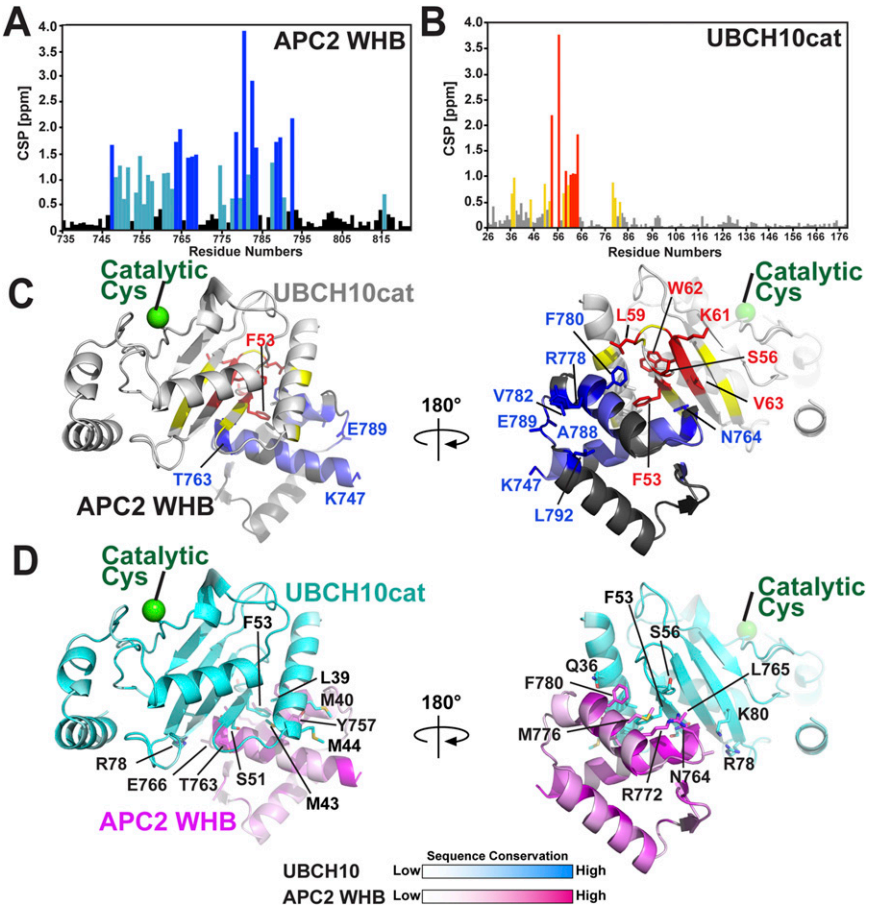

Fig. S7. NMR studies of APC2^{W}–UBCH10^{cat} interactions. (*A*) NMR chemical shift perturbations (CSPs) for APC2^{W} when bound to UBCH10^{cat} of <0.5, 0.5–1.5, or >1.5 ppm are shown in black, cyan, and navy, respectively. (*B*) CSPs for UBCH10^{cat} when bound to APC2^{W} of <0.5, 0.5–1.0, or >1.0 ppm are shown in gray, yellow, or orange, respectively. (*C*) Crystal structure of APC2^{W}–UBCH10^{cat} with residues colored by degree of CSP upon complex formation indicated in *A* and *B*. (*D*) Crystal structure of APC2^{W}–UBCH10^{cat} with residues colored by sequence conservation using ProtSkin (1). UBCH10^{cat}: no conservation, white; 100% conserved, cyan. APC2^{W}: no conservation, white; 100% conserved, magenta.

1. Ritter B, et al. (2004) Two WXXF-based motifs in NECAPs define the specificity of accessory protein binding to AP-1 and AP-2. *EMBO J* 23(19):3701–3710.

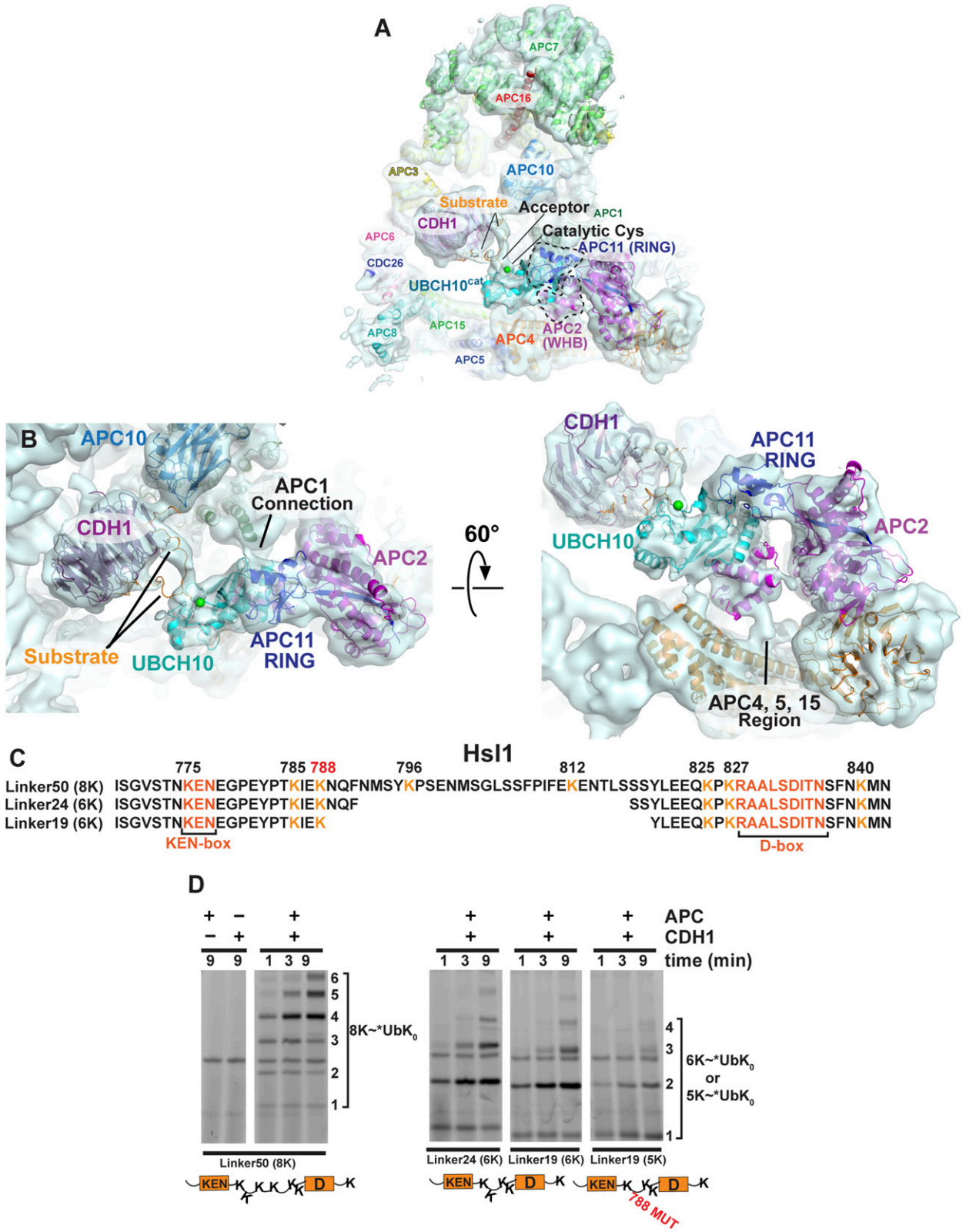

Fig. S8. Lysine prioritization in APC substrates defined by APC^{CDH1} mechanism of UBCH10 recruitment. (*A*) Cryo-EM reconstruction of the APC^{CDH1}–UBCH10–Ub–substrate complex, showing APC2^{W}–UBCH10^{cat} structure docked with APC11 RING domain fit into the EM map using Chimera (1), along with nearly complete secondary structure model of other APC subunits. (*B*) Juxtaposition of substrate and UBCH10~Ub through multisite recruitment. (*Left*) Close-up of cryo-EM map for the APC^{CDH1}–UBCH10–Ub–substrate complex, highlighting multisite recruitment of a substrate (Hsl1^{P}, orange) to CDH1 (purple) and APC10 (light blue). (*Right*) Close-up of cryo-EM map for the APC^{CDH1}–UBCH10–Ub–substrate complex, highlighting multisite recruitment clamping UBCH10 (cyan) via interactions with the WHB domain from APC2 (magenta) and the RING domain from APC11 (navy). Notably, the position of the catalytic assembly may be

Legend continued on following page

restrained by the N terminus of UBCH10, the RING domain, and APC2's WHB domain (below the plane of the image) approaching APC1 on one side (highlighted in left panel), and by contacts between APC2's WHB domain and UBCH10 and the APC4/APC5/APC15 region on the other (shown on *Right*). (*C*) Sequences of peptides derived from APC substrate Hsl1 with different linker lengths between the KEN- and D-box. These were tested as substrates for ubiquitination by APC^{CDH1} and UBCH10. Each Hsl1 variant peptide is labeled with the amino acid length between the KEN- and D-boxes (Linker50 has 50 residues between the KEN- and D-boxes, Linker24 has 24 residues between the KEN- and D-boxes, Linker19 has 19 residues between the KEN- and D-boxes) along with the number of lysines (orange) available for modification (8K has 8 lysines, 6K has 6 lysines, or 5K has 5 lysines). (*D*) Fluorescence scan of SDS/PAGE gel monitoring APC^{CDH1} and UBCH10-catalyzed modification of Hsl1 variants with fluorescently labeled UbK_0. The length of the linker between the KEN- and D-box presumably dictates ability to access E2 active site, and the number of lysines influence the number of substrate modifications in the assay. Evidence for lysine prioritization is also indicated by reduced ubiquitination of Linker19 Hsl1 harboring a Cys replacement for the preferred target (Lys788) identified in Fig. S1. Linker 19 with azidohomoalanine in place of Lys788 is $Hsl1^{P}$ used to generate three-way crosslinked UBCH10-Ub-Substrate complex for EM. This assay was performed by mixing 50 nM E1 (UBA1), 100 nM UBCH10, 250 nM APC–CDH1, 1 μM Hsl1 variant peptide, and 5 μM $*UbK_0$ at room temperature for the indicated times.

1. Pettersen EF, et al. (2004) UCSF Chimera—a visualization system for exploratory research and analysis. *J Comput Chem* 25(13):1605–1612.

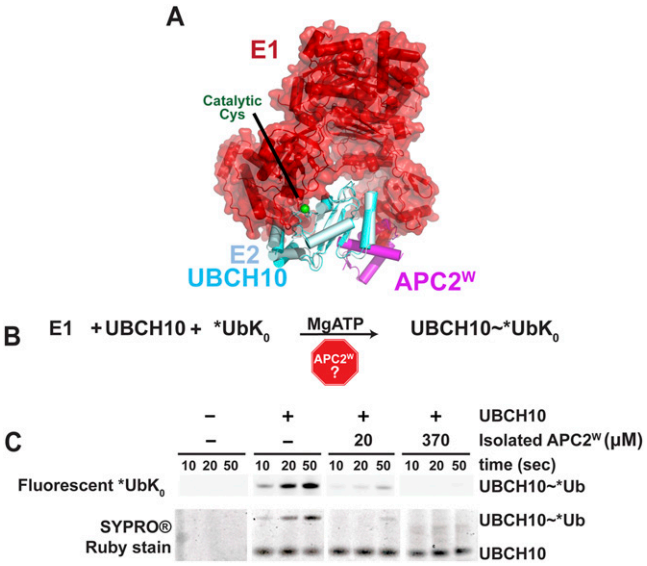

Fig. S9. Mutually exclusive UBCH10 recruitment to APC and Ub loading by E1. (*A*) Structural superposition of E2s from $APC2^{W}$ (magenta)–$UBCH10^{cat}$ (cyan) crystal structure with prior structure of an E1 (red)–E2 (pale cyan) complex (4II2.pdb) (1) shows that UBCH10's E1 and $APC2^{W}$-binding surfaces would overlap. (*B*) Scheme for assay testing whether UBCH10 binding to E1 and $APC2^{W}$ is mutually exclusive. E1 (UBA1)-catalyzed loading of UBCH10 with lysineless Ub ($*UbK_0$) was examined in the absence or presence of isolated $APC2^{W}$ domain. (*C*) Fluorescence ($*UbK_0$) and SYPRO Ruby detection (UBCH10 and $*UbK_0$) from SDS/PAGE gels of experiment described in *B*. $APC2^{W}$ prevents UBCH10 from being loaded with $*UbK_0$ by E1.

1. Olsen SK, Lima CD (2013) Structure of a ubiquitin E1-E2 complex: Insights to E1-E2 thioester transfer. *Mol Cell* 49(5):884–896.

Table S1. Crystallographic data and refinement statistics

	$APC2^{W}$–$UBCH10^{cat}$
Data collection	
Beam line	NECAT 24-ID-C
Space group	C2
Unit cell parameters	
a, *b*, *c*, Å	133.1, 33.2, 52.0
α, β, γ, °	90, 100, 90
Resolution, Å (highest shell)	50–1.8 (1.86–1.8)
Wavelength, Å	1.2826
No. of measured reflections	248,711
No. of unique reflections	21,055
Overall R_{sym}	0.05 (0.347)
Completeness, %	94 (68.2)
Overall $I/\sigma I$	28.4 (1.9)
Multiplicity	2.9 (2.3)
Refinement	
Resolution, Å	44–1.8
R_{work}/R_{free}	0.1963/0.2454
Rmsd bond lengths, Å	0.013
Rmsd bond angles, °	1.499
No. of atoms	
Proteins	1,704
Ramachandran statistics	
Favored, %	97.2
Allowed, %	2.8
Outliers, %	0